AWARD NUMBER: W81XWH-18-1-0628

TITLE: Longitudinal Analysis of Disease Site Activities Impairing Wound Healing in Epidermolysis Bullosa and Development of Therapeutic Strategies

PRINCIPAL INVESTIGATOR: Dr. Olga Igoucheva, Ph.D.

CONTRACTING ORGANIZATION: Thomas Jefferson University

REPORT DATE: September 2020

TYPE OF REPORT: Annual

PREPARED FOR: U.S. Army Medical Research and Development Command
Fort Detrick, Maryland 21702-5012

REPORT DOCUMENTATION PAGE

Form Approved
OMB No. 0704-0188

1. REPORT DATE	2. REPORT TYPE	3. DATES COVERED
September 2020	Annual	1 Sep 2019 – 31 Aug 2020

4. TITLE AND SUBTITLE

Longitudinal Analysis of Disease Site Activities Impairing Wound Healing in Epidermolysis Bullosa and Development of Therapeutic Strategies

5a. CONTRACT NUMBER
W81XWH-18-1-0628

5b. GRANT NUMBER
PR170101

5c. PROGRAM ELEMENT NUMBER

6. AUTHOR(S)

Dr. Olga Igoucheva, Ph.D.

E-Mail: Olga.Igoucheva@jefferson.edu

5d. PROJECT NUMBER

5e. TASK NUMBER

5f. WORK UNIT NUMBER

7. PERFORMING ORGANIZATION NAME(S) AND ADDRESS(ES)

Thomas Jefferson University
Philadelphia, Pennsylvania 19107-5567

8. PERFORMING ORGANIZATION REPORT NUMBER

9. SPONSORING / MONITORING AGENCY NAME(S) AND ADDRESS(ES)

U.S. Army Medical Research and Development Command
Fort Detrick, Maryland 21702-5012

10. SPONSOR/MONITOR'S ACRONYM(S)

11. SPONSOR/MONITOR'S REPORT NUMBER(S)

12. DISTRIBUTION / AVAILABILITY STATEMENT

Approved for Public Release; Distribution Unlimited

13. SUPPLEMENTARY NOTES

14. ABSTRACT

Poorly healing wounds are one of the major complications in patients suffering from recessive dystrophic epidermolysis bullosa (RDEB). At present, there are no effective means to analyze changes in cellular and molecular networks occurring during RDEB wound progression to predict wound outcome and design betted wound management approaches. To better define mechanisms influencing RDEB wound progression by evaluating changes in molecular and cellular networks. We developed a non-invasive approach for sampling and analysis of wound-associated constituents using wound-covering bandages. Cellular and molecular components from seventy-six samples collected from early, established and chronic RDEB wounds were evaluated by FACS-based immuno-phenotyping and ELISA. Our cross-sectional and longitudinal analysis determined that progression of RDEB wounds to chronic state is associated with the accumulation (up to 90%) of $CD16^+CD66b^+$ mature neutrophils, loss of $CD11b^+CD68^+$ macrophages, and a significant increase (up to 50%) in a number of $CD11c^+CD80^+CD86^+$ activated professional antigen presenting cells (APC). It was also marked by changes in activated T cells populations including a reduction of $CD45RO^+$ peripheral memory T cells from 80% to 30% and an increase (up to 70%) in $CD45RA^+$ effector T cells. Significantly higher levels of MMP9, VEGF-A and cathepsin G were also associated with advancing of wounds to poorly healing state. Our data demonstrated that wound-covering bandages are useful for a non-invasive sampling and analysis of wound-associated constituents and that transition to poorly healing wounds in RDEB patients as associated with distinct changes in leukocytic infiltrates, matrix-remodeling enzymes and pro-angiogenic factors at wound sites.

15. SUBJECT TERMS

Epidermolysis Bullosa, wound healing, microbiome

16. SECURITY CLASSIFICATION OF:			17. LIMITATION OF ABSTRACT	18. NUMBER OF PAGES	19a. NAME OF RESPONSIBLE PERSON
a. REPORT	b. ABSTRACT	c. THIS PAGE			USAMRMC
Unclassified	Unclassified	Unclassified	Unclassified	17	19b. TELEPHONE NUMBER *(include area code)*

Standard Form 298 (Rev. 8-98)
Prescribed by ANSI Std. Z39.18

TABLE OF CONTENTS

Page

1. INTRODUCTION

Epidermolysis bullosa (EB), a heterogeneous group of mechanobullous disorders, is characterized by fragility of the skin. Tissue separation manifesting as blistering of the skin and mucous membranes in different variants of EB takes place at the level of the cutaneous basement membrane zone (BMZ) at the dermal-epidermal junction (DEJ). Despite extensive studies of EB genetics and testing various therapeutic approaches to cure the disease, only palliative care revolving around judicious use of protective garments, bandages, and antibiotic creams is available to EB patients. Separation of skin layers following minor trauma to the skin is a hallmark of the disease. It leads to the development of blisters, erosions and non-healing wounds, which are associated with numerous complications including infection, sepsis, dehydration, deformities, and cancer. Although many EB skin blisters and erosions progress to skin wound, at present, there is no objective measure to predict whether a wound will heal or become chronic. Our previous findings indicate that blistering and wounded EB skin is characterized by an excessive production of several pro-inflammatory chemokines and deregulated recruitment of the leukocytes, particularly neutrophils, to the damaged skin. This is accompanied by the activation of adaptive and innate immunity triggered by wound colonizing bacteria and release of extracellular matrix (ECM) remodeling enzymes from the recruited neutrophils. In turn, secreted enzymes in blister fluids and wounds continuously degrade ECM and generate ECM-derived damage associated molecular patterns (DAMPs) that activate toll-like receptors (TLRs) on fibrocytes, and create a pro-inflammatory feedback loop. In case of a skin injury, when physical segregation between the host and microbiota is destroyed, the immune system could be overwhelmed by the volatile situation - when pathogens and commensals share the same inflamed environment and may negatively affect wound heling, particularly in EB-affected skin compromised by the abnormal DEJ. As adequate T cell responses are essential for immune-mediated protection against microbiota, we suggest that a high number of activated T cells at wound sites can either exhaust or establish tolerance toward wound-colonizing bacteria. Together, these events create a favorable milieu for the persistent inflammation, excessive digestion of the ECM, abrogation of keratinocyte motility, wound re-epithelization, and fibrosis. To date, no study has investigated these dynamics in EB blisters and wounds. Our current studies are designed to assess the complexity of the molecular and cellular interactions influencing the development of non-healing wounds on EB genetic background, and to delineate therapeutic intervention approaches. During first year of the project, we leveraged the ability of our clinical collaborator, Dr. J. Salas, to follow particular wounds on patients affected by different EB types while providing standard of care and our capacity to characterize healing capacities of EB-associated wounds on different genetic backgrounds. In addition, to define microbial biomarkers predictive of the wound outcome, we initiated studies on the dynamics of bacterial and fungal communities during wound progression and healing. Ultimately, these studies will allow us to delineate molecular and cellular activities/mechanisms, which inhibit wound healing process.

2. KEYWORDS

EB - Epidermolysis Bullosa
EBS - Simplex Epidermolysis Bullosa
JEB - Junctional Epidermolysis Bullosa
DEB - Dystrophic Epidermolysis Bullosa
ECM - Extracellular Matrix
BMZ - Basement Membrane Zone
DAMPs - Damage Associated Molecular Patterns
ELR - Glu-Leu-Arg (ELR) Motif
TLRs - Toll-like Receptors
BF - Blister Fluids
FnEDA - Fibronectin Extra Domain A
APC - Antigen Presenting Cells
Ag - Antigens
CTL - Cytotoxic T Lymphocytes
PBMC - Peripheral Blood Mononuclear Cells

FACS - Fluorescence Activated Cell Sorting
ELISA - Enzyme-linked Immunosorbent Assay
HMW - High Molecular Weight
LMW - Low Molecular Weight

3. OVERAL PROJECT SUMMARY

Poorly healing wounds are one of the major complications in patients suffering from epidermolysis bullosa (EB). At present, there are no effective means to analyze changes in cellular and molecular networks occurring during EB wound progression to predict wound outcome and design betted wound management approaches. To better define mechanisms influencing EB wound progression by evaluating changes in molecular and cellular networks. We developed a non-invasive approach for sampling and analysis of wound-associated constituents using wound-covering bandages. Cellular and molecular components from seventy-six samples collected from early, established and chronic EB wounds were evaluated by FACS-based immuno-phenotyping and ELISA. Our cross-sectional and longitudinal analysis determined that progression of RDEB wounds to chronic state is associated with the accumulation (up to 90%) of $CD16^{+}CD66b^{+}$ mature neutrophils, loss of $CD11b^{+}CD68^{+}$ macrophages, and a significant increase (up to 50%) in a number of $CD11c^{+}CD80^{+}CD86^{+}$ activated professional antigen presenting cells (APC). It was also marked by changes in activated T cells populations including a reduction of $CD45RO^{+}$ peripheral memory T cells from 80% to 30% and an increase (up to 70%) in $CD45RA^{+}$ effector T cells. Significantly higher levels of MMP9, VEGF-A and cathepsin G were also associated with advancing of wounds to poorly healing state. Our data demonstrated that wound-covering bandages are useful for a non-invasive sampling and analysis of wound-associated constituents and that transition to poorly healing wounds in EB patients as associated with distinct changes in leukocytic infiltrates, matrix-remodeling enzymes and pro-angiogenic factors at wound sites.

4. KEY RESEARCH ACCOMPLISHEMNTS

Specific Aim 1. To conduct longitudinal analysis of secretome in epidermolysis bullosa (EB) healing and non-healing wounds and define the role of leukocytic and fibrocytic infiltrates.

Major Task 1: Cross-sectional and longitudinal evaluation of secretome in healing and non-healing EB wounds.

Subtask 1: **S**ample collection and evaluation of wounds in EB-affected patients. Timeline - 18 months (1-18).
Per SOW: Wound-dressing bandages will be collected during routine re-dressing of the wounds at Dr. Salas's clinique. Demographic data, EB type, age of the wound will be collected by attending physicians at Dr. Salas's clinique. At least 40 patients with each type of wound (fresh, established or chronic) will be used for cross-sectional analysis. At least 40-50 patients with each type of wound (fresh, established or chronic) will be used for longitudinal analysis with 8 to 12 repeated measures per wound during the observation period of about one year and a half. To rigorously investigate any potential sex bias, all experiments will be done in male and female cohorts.
Progress: As the most essential component of the project is samples (wound-covering bandages and swabs) from patients suffering with various forms of EB, we established very close interaction/collaboration with the clinician in EB area, Dr. Julio Salas (Mexico). Wound-dressing bandages (at least 80) and wound swabs were collected during routing re-dressing of the wounds at Dr. Salas's clinic. Demographic data, EB type, state of the wound were documented by attending physicians at Dr. Salas's clinic. To rigorously investigate any potential sex bias, all experiments were done in male and female cohorts. As a majority of EB patients uses regular gauze, all samples were normalized with regard to wound dressing material. Clinician also documented use of petroleum gel or Mupirocin cream (for chronic wounds). During each visit, the patients were asked to describe the natural history of each sampling site. Also, at each visit, wounds were coded and documented by description to include body site, antibiotic treatment (local or systemic), other drugs received and creams applied, as well as overall appearance of the wound. Gauze (bandage) directly exposed to the wound bed was excised by attending

physician, placed into a tube with transport media supplemented with Penicillin/Streptomycin/Amphotericin B and sent to the Dr. Igoucheva's laboratory. Upon arrival to the laboratory, bandages were immediately processed for the isolation of cellular and secreted components. Briefly, bandage-harbored cells were collected by scraping and centrifugation using aseptic techniques in the tissue culture hood. Resultant cell pellets were partially used for immediate FACS analysis and frozen cell stocks were made for future assays. Our established protocol permitted the retrieval on average $1x10^6$ - $6x10^6$ cells from a single bandage with an equal distribution (50/50) of leukocytic and fibroblastoid infiltrates.

Subtask 2: Analysis of secretome activity in early, established and chronic wounds. Timeline - 18 months (1-18).
Per SOW: Bandage transport media from wound dressings will be collected, clarified and concentrated for secretome analysis. Composition of EB secretomes will be evaluated by Multiplex ELISA assays. Secretome activity of various EB wounds on recruitment of various inflammatory cells will be evaluated using various FACS-based protocols.
Progress: Bandage transport media from wound dressings was collected, clarified and concentrated for secretome analysis. Transport media was clarified by filtration on 0.22 microns filters, and subsequently concentrated on a 100 kDa cut-off centrifugal device to obtain a high molecular weight (HMW) fraction and a 10 kDa Amicon filter fraction (low molecular weight (LMW) fraction). Concentrated LMW fractions were stored at -80^0 C for the assessment of the secretome by Multiplex ELISA assay, whereas HMW fractions were stored at -80^0 C for the analysis of larger molecules (e.g. fibronectin extra domain A, FnEDA) by Western blot analysis. Composition of EB secretomes was further evaluated by Multiplex ELISA assays.

Using LegendPlex approach, we compared the secretory profiles of numerous molecules ascribing distinct cytokine and chemokine signatures to physiological and pathological wound healing. The presence and quantity of 13 chemokines (LegendPlex Human Inflammatory Panel), 13 cytokines (LegendPlex Human Pro-Inflammatory Panel), 13 Th cytokines (LegendPlex Human Th Panel), and 13 growth factors (LegendPlex Human Growth Factors Panel) in LMW material were assessed against known concentrations of analytes using bead-based multiplex assays according the vendor's instructions. At least 5000 beads per analyte were acquired utilizing a Guava easyCyte flow cytometer (available in the laboratory). Curve fitting of the standards' mean fluorescence intensities and quantitative calculation of the samples' mean fluorescence intensities to pg/mL was achieved utilizing LegendPlex software. Statistical analysis was carried out using *Prism* 7.01 (GraphPad software, La Jolla, CA, USA). We applied multiple *t* tests with Holm-Sidak correction for multiple comparison with an α=.05 to statistically compare the concentration of a given molecule in various samples for each analyte independently. The presence and regulation of a number of prominent wound regulators such as IL-6, IL-8, IL-18, EGF, VEGF and PDGF have been reported in previous studies, suggesting our experimental approach to be valid (Table 1). Also, we identifed an increase in TNF-α or TGF-α as previously seen in chronic wounds. The concentrations of GROα and MCP-1, important during the inflammatory phase, were significantly different between chronic and early wounds. Intriguingly, we found a number of molecules that have yet not been frequently reported to be differentially expressed in chronic and/or diabetic in comparison with acute wounds. Interestingly, leucocyte-attracting RANTES (CCL5), which is negatively regulated by nitric oxide (NO) during the early inflammatory phase to initiate wound repair, was steadily present in all samples. Chronic wounds are rich in senescent neutrophils and lymphocytes, and their presence together with a sustained release of NO may have negatively regulate RANTES expression, yet without positive consequences for wound healing. Also level of I-TAC (CXCL11), a keratinocyte and endothelial cell-derived chemokine functioning in an autocrine/paracrine fashion in wound repair, was strongly downregulated in established and chronic wounds. This may reflect the wound not successfully transitioning to the proliferative phase as CXCL11-expressing cells are present at T-cell infiltrates in various human skin diseases, suggesting a mislead inflammation that is also known to be detrimental in healing. IL-17 and IL-23 were significantly down-regulated in chronic wounds. Both molecules were shown to be important in distorted inflammation. Considering their parallel regulation, M1 macrophage-derived IL-23 drives inflammation via IL-17 and Th17 induction in many diseases. IP-10 was also downregulated in chronic wounds. In normal wound healing, it parallels lymphocyte immigration, and serves a role in dermal remodeling, for example via inhibition of fibroblast migration, and is angiostatic. Collectively,

the presence and/or aberrant regulation of a number of well-known molecules was confirmed such as IL-6, IL-8, IL-18, PDGF, VEGF, EGF, TGF-α, and bFGF. Importantly, we identified significantly different expression levels between different wound states for *hitherto* less reported molecules in the context of defective wound healing, such as RANTES, I-TAC, IL-17A, IL-23, HGF, and IP-10. The results underline the high complexity of the chronic wound environment and may help to put past and future work in further perspective.

Table 1. LegendPlex (Multiplex ELISA)-based Heatmap of absolute concentrations of selected analytes in EB patient samples taken from wounds at different stage of wound progression.

Human Inflammation	IL-1β	IFN-α2	IFN-γ	TNF-α	MCP-1	IL-6	IL-8	IL-10	IL-12p70	IL-17A	IL-18	IL-23	IL-33
Blister Fluids	95	69	72	480	243	2958	785	100	0	41	132	0	423
Early	30508	13	188	155	643	1170	790	267	0	19	702	0	338
Established	45049	33	66	175	1898	2417	464	181	51	41	231	89	769
Chronic	2063	284	213	97	639	6211	660	68	0	34	497	0	289

Human Th 13 Plex	IL-5	IL-13	IL-2	IL-6	IL-9	IL-10	IFN-γ	TNF-α	IL-17A	IL-17F	IL-4	IL-21	IL-22
Blister Fluids	0	48	56	2109	80	31	0	0	43	95	24	83	24
Early	0	0	0	1406	80	121	538	1963	47	360	0	0	32
Established	0	0	0	2786	61	58	774	821	172	173	0	0	79
Chronic	0	0	0	2420	0	35	0	425	57	70	0	0	35

Human Growth Factors	Angiopoietin-2	EGF	EPO	FGF-basic	G-CSF	GM-CSF	HGF	M-CSF	PDGF-AA	PDGF-BB	SCF	TGF-α	VEGF
Blister Fluids	1509	53	352	609	775	564	1702	316	153	539	326	709	588
Early	1669	7517	193	0	782	0	2779	404	207	0	0	418	738
Established	785	5870	280	0	1739	205	3558	244	174	0	0	601	894
Chronic	503	8011	0	0	1601	0	4291	142	90	0	0	599	1133

Human Pro-Inflammatory Cytokines	IL-8	IP-10	Eotaxin	TARC	MCP-1	RANTES	MIP-1α	MIG	ENA-78	MIP-3α	GROα	I-TAC	MIP-1β
Blister Fluids	8408	6127	238	1594	3520	238	1237	1309	289	746	479	229	109
Early	48631	153	225	0	1575	350	1447	1744	192	107	613	121	126
Established	50702	254	239	92	2429	191	1572	924	200	150	506	0	143
Chronic	42256	105	229	0	679	310	1183	1215	216	125	1007	0	99

Analytes were sorted according to their *P*-value.

Milestone(s) Achieved: Timeline - 18 month. A well characterized analysis of secretome of EB-associated wounds. Acquisition of statistically significant data. All tasks are accomplished, manuscript in preparation.

Major Task 2: Cross-sectional and longitudinal analyses of cellular infiltrates in EB healing and non-healing wounds

Subtask 1: Characterization of cellular infiltrates at the sites of healing and non-healing EB skin wounds. Timeline - 18 months (1-18).
Per SOW: Wound-associated bandage-derived cells will be isolated concurrently with the secretome using cell-specific techniques. Evaluation of wound-associated cell populations will be done using FACS-based protocols.

Progress: During our studies, we developed a non-invasive approach for isolation of wound bed-associated cells for analysis of inflammatory infiltrates at different stages of wound progression. While establishing recovery protocol, we noted that cells isolated from bandages stayed on the wounds for 24-48 h show 3-4

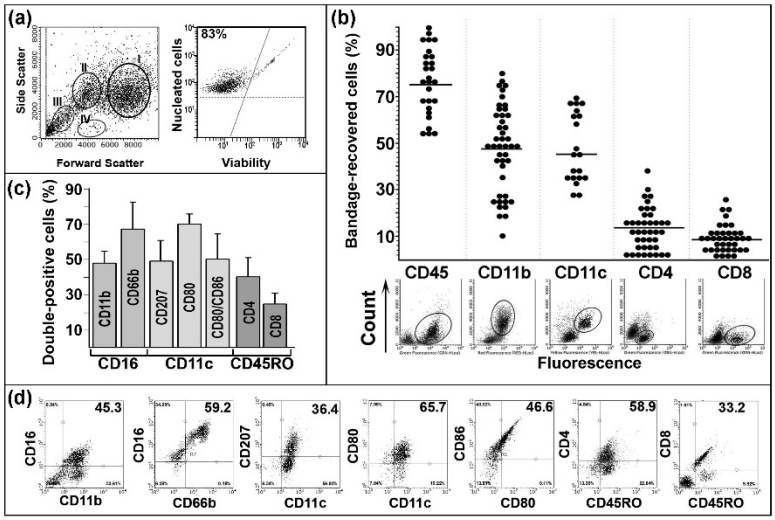

Fig. 1. FACS-based analysis of bandage-recovered cellular constituents of RDEB wounds. (**a**) Scatter plot evaluation of cellular populations. Roman numerals mark populations of distinct size and complexity. Percentage of viable cells recovered from bandages is shown in the upper left quadrants of the viability plot. (**b**) Dot-plot evaluation of bandage-recovered cells expressing specific leukocytic markers, as indicated below the plots. Each dot represents an average of duplicate measures per individual sample. Number of dots corresponds to a number of bandages used in the analysis. Annotated bars show mean percentages of marker-specific cells. Representative scatter plots with outlined marker-specific populations are shown below the dot plots. (**c**) Columns showing mean percentages of marker-specific populations ±SD defined by staining with subset-specific markers shown on and under the columns. (**d**) Representative scatter plots showing distribution and percentages (upper right quadrant) of specific subsets in bandage-recovered leukocytes. Detected antigens are shown to the left and under the corresponding plots. In all scatter plots, detected antigens are shown on axes. Percentages of double-positive cells are shown in upper right quadrants.

distinct cell populations of varying sizes and complexity, with an average viability of 80% (Fig. 1a). Fluorescence activated cell sorting (FACS)-based immuno-phenotyping showed that on average 75% of recovered cells were represented by $CD45^+$ cells (Fig. 1b). Gating on specific populations showed that population I and IV were mostly comprised of $CD45^+$ leukocytes, presumably myeloid and T cells, respectively. The remaining 25% of $CD45^-$ bandage-associated cells were mostly represented by fully differentiated and anucleated keratinocytes (population II) (Fig. 5c). Bandage-recovered cells associated with population III were able to produce fibroblastic cell cultures, which differentiate into alpha smooth muscle actin (αSMA) expressing cells when maintained as a sparse culture (Fig. 5d-g). Further immuno-phenotyping showed that about 47% of leukocytes expressed CD11b myeloid cell marker, 45% of CD11c antigen presenting cell (APC) marker, and about 10% expressed CD8 and CD4 T cell markers (Fig. 1b). About 50% of $CD11b^+$ cells expressed CD16 myeloid cell marker, and about 70 % of these cells were positive for CD66b granulocyte neutrophil activation marker (Fig. 1c, d). In addition, 49% of $CD11c^+$ expressed CD207 (Langerin) marker of Langerhans cells (LC). On average, 70% of all $CD11c^+$ cells expressed CD80 APC activation marker, 50% of which co-express CD86. Activated/effector populations were noted in $CD4^+$ and $CD8^+$ bandage-derived T cells. Cumulative data showed that about 40% of $CD4^+$ and 25% of $CD8^+$ T cells express CD45RO marker of antigen-experienced effector memory T cells (Fig. 1c, d). About 60% of $CD4^+$ and 75% of $CD8^+$ cells expressed CD45RA marker of naïve and effector cells (data not shown).

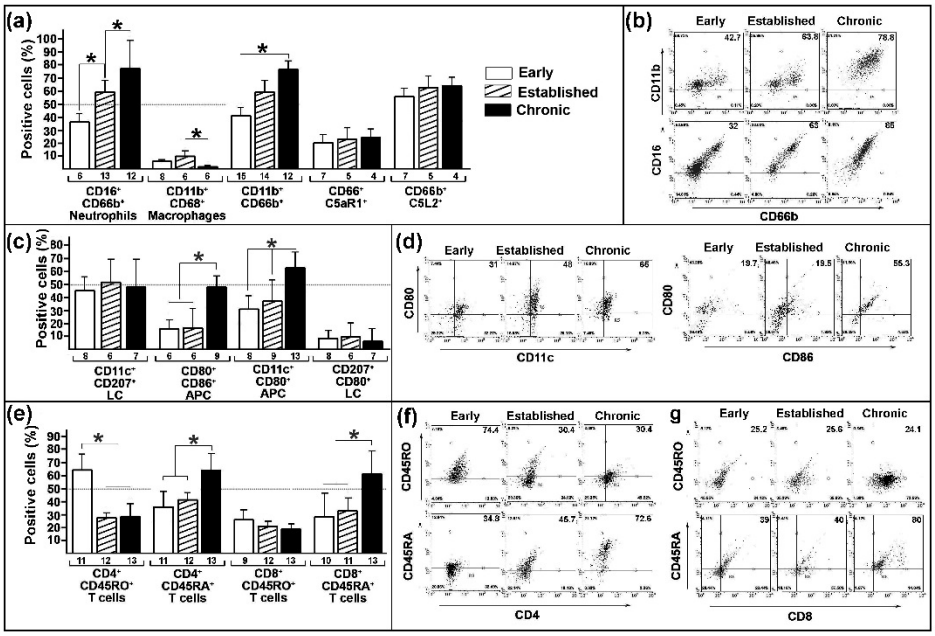

Considering broad distribution of $CD11b^+$, $CD11c^+$, and T cell populations in bandage-derived cells (Fig. 1b), we further investigated whether percentages of specific cell types correlate with wound progression. All wounds were categorized into three groups, early, established and chronic, as defined by the age of the wounds reported by the patients or their care persons, and association of specific sets of leukocytes within these wounds was analyzed. FACS-based evaluation

Fig. 2. FACS analysis of specific cellular subsets in RDEB wounds. (**a**) Column charts and (**b**) representative density pots illustrating progressive accumulation of $CD16^+CD66b^+$ and $CD11b^+CD66b^+$ mature neutrophils and dissipation of $CD11b^+CD68^+$ macrophages in chronic wounds. (**c**) Column charts and (**d**) representative density plots illustrating accumulation of $CD11c^+CD80^+CD86^+$ APC in chronic wounds. (**e**) Column charts and (**f, g**) representative density pots depicting reduction of $CD45RO^+CD4^+$ and $CD8^+$ peripheral memory T cells and accumulation of $CD45RA^+$ effector T cells in chronic wounds. Wound type (early, established, chronic) is indicated in the key in panel (**a**). In all column charts, detected antigens are shown below the columns. Y-axis: percent of double-positive cells. The data are presented as mean percentage ±SD. Statistical significance ($p<0.05$) is indicated by asterisk. Number of analyzed bandages per wound type per combination of antigens is shown under the columns. In all scatter plots, detected antigens are shown on axes. Percentages of double-positive cells are shown in upper right quadrants.

showed a progressive and significant accumulation of $CD11b^+CD66b^+$ cells at chronic wounds. In early wounds, neutrophils represented about 20% of total leukocytes, whereas in 3 weeks and older wounds these cells represented up to 90% of total leukocytes (Fig. 2a, b). Further immuno-phenotyping confirmed that this population is represented by $CD16^+CD66b^+$ mature neutrophils (Fig. 2b). Accumulation of neutrophils in chronic wounds could be associated with dysfunctional healing and correlate with the loss of complement component 5a C5aR1 and C5L2 receptors. However, examination of 5a C5aR1 and C5L2 expression on $CD66b^+$ cells showed no significant reduction of both receptors on neutrophils recovered from either early or chronic wounds. FACS-based evaluation showed that an average 60% and 20% of $CD66b^+$ neutrophils express C5L2 and C5aR1 receptors, respectively, in all wound types (Fig. 2a). Interestingly, $CD11b^+CD68^+$ macrophages were present at low fractions in all examined wounds (Fig. 2a). Overall percentage of macrophages among wound-bed associated leukocytes was higher in established wounds (up to 10%) but dropped significantly down to 2.5% in chronic wounds (Fig. 2a). All $CD11c^+$ APC were equally represented by $CD207^+$ LC and $CD207^-$ DC populations in all wound types (Fig. 2c). Intriguingly, progression of wounds from early to chronic was associated with the accumulation of $CD11c^+CD80^+$ activated APC. Early wounds contained about 30% of $CD80^+$ APC, whereas chronic wounds showed up to 70% of activated APC (Fig. 2c, d). In all wound types, there were no significant changes in $CD207^+$ LC activation. These findings were further confirmed by evaluation of both CD80 and CD86 activation markers. About 17% of total APC expressed both makers in early and established wounds, while this percentage was increased up to 35% in chronic wounds. These data showed that accumulation of the activated APC in chronic wounds is mostly due to the accumulation of activated DC. Evaluation of the T cells showed that early wounds were populated with $CD4^+CD45RO^+$ effector memory and $CD4^+CD45RA^+$ naïve T cells (Fig. 2e-g). Progression of wounds was associated with a substantial decrease of the effector memory T cells and increase of the $CD4^+CD45RA^+$ effector T cells in chronic wounds (Fig. 2c). Similar trend was observed for $CD8^+$ T cells.

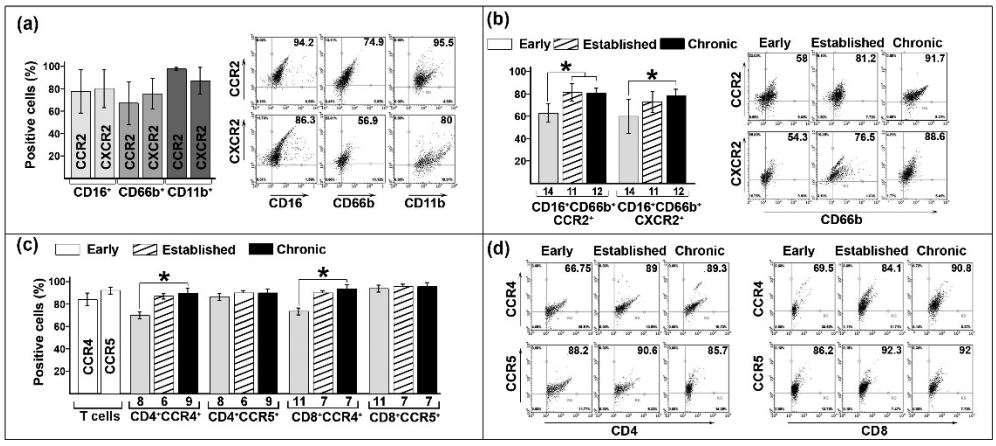

Fig. 3. FACS analysis of chemokine receptors on RDEB wound-associated leukocytes. (**a**) Column charts and representative profiles depicting expression of CXCR2 and CCR2 chemokine receptors on $CD16^+$, $CD66b^+$, and $CD11b^+$ myeloid cell populations. Detected chemokine receptors are on the columns. (**b**) Column charts and representative profiles depicting CCR2 and CXCR2 expression on $CD16^+CD66b^+$ mature neutrophils in early, established and chronic wounds. (**c**) Column charts illustrating expression of CCR4 and CCR5 chemokine receptors on a total population of wound-associated T cells and on $CD4^+$ and $CD8^+$ T cells in early, established and chronic wounds. (**d**) Representative density plots depicting CCR4 and CCR5 expression of CD4 and CD8-gated T cell populations in early, established and chronic wounds. In all column charts, the data are presented as mean percentage ±SD. Statistical significance ($p<0.05$) is indicated by asterisk. Number of analyzed bandages per wound type per combination of antigens is shown under the columns. In all scatter plots, detected antigens are shown on axes. Percentages of double-positive cells are shown in upper right quadrants.

Previously we published that high levels of CCR2, CXCR1, CXCR2, and CCR4 ligands dominate early RDEB blisters, and that these chemokine receptors support directional migration of leukocytes *in vitro*. Evaluation of these receptors on bandage-derived leukocytes showed that about 80% of cells expressed both CCR2 and CXCR2 receptors (Fig, 3a, b). Most consistent receptor expression was detected on CD11b-gated cell population. Substantially greater variations in percentages of $CCR2^+$ cells were seen in CD66b-gated cells. Nevertheless, analysis of $CD66b^+$ population showed a significant accumulation of both $CCR2^+$ and $CXCR2^+$ cells in established and chronic wounds (Fig. 3a, b). Previously, we also reported that $CCR4^+$ and $CCR5^+$ lymphocytes migrate in response to RDEB-derived blister fluids *in vitro*. As an accumulation of the activated/effector T cells was observed in chronic wounds, we evaluated whether these chemokine receptors could facilitate migration of the T cells to the wound bed. When assessing a T-cell gated population, about 83% and 91% of cells were identified as $CCR4^+$ and $CCR5^+$, respectively. Percentages of $CCR5^+$ T cells (both $CD4^+$ and $CD8^+$) were consistently high in all wound types (Fig. 3c, d). In early wounds, about 70% of $CD4^+$ and 86% of $CD8^+$ T cells express CCR4 on cell surface. In established and chronic wounds, these percentages were significantly increased up to 86% and 91%, respectively (Fig. 3c, d).

Wound repair results from a highly complex interaction of cellular and biochemical events. Yet, these molecular networks remain poorly defined in RDEB wounds. Here, we tested whether wound-covering bandages could be used for a non-invasive evaluation of wound-associated soluble molecules. Considering a known contribution of matrix metalloproteinases (MMPs) to chronic wound pathogenesis, we assessed several MMPs, including MMP2 and MMP9, in a low molecular weight (LMW) fraction collected from different wounds. Quantitative cytokine-specific ELISA showed that both MMPs are present at wound sites, and that concentration of MMP9 is 5-10 times greater than MMP2. Moreover, significantly higher MMP9 levels were detected in established and chronic wounds as compared to early lesions (Fig. 4a). Consistent with our prior studies, we also detected low levels of tissue inhibitor of metalloproteinases 1 (TIMP-1) in all wounds. When evaluating MMP9/TIMP-1 ratio, another predictor of wound healing [11], we found that early RDEB wounds had the highest MMP9/TIMP-1 ratio (Fig. 4b). Considering that mature neutrophils produce MMPs and other matrix remodeling enzymes, we also assessed cathepsin G content. Concentration of this serine protease was significantly higher in chronic RDEB wounds as compared to early wounds (Fig. 4c).

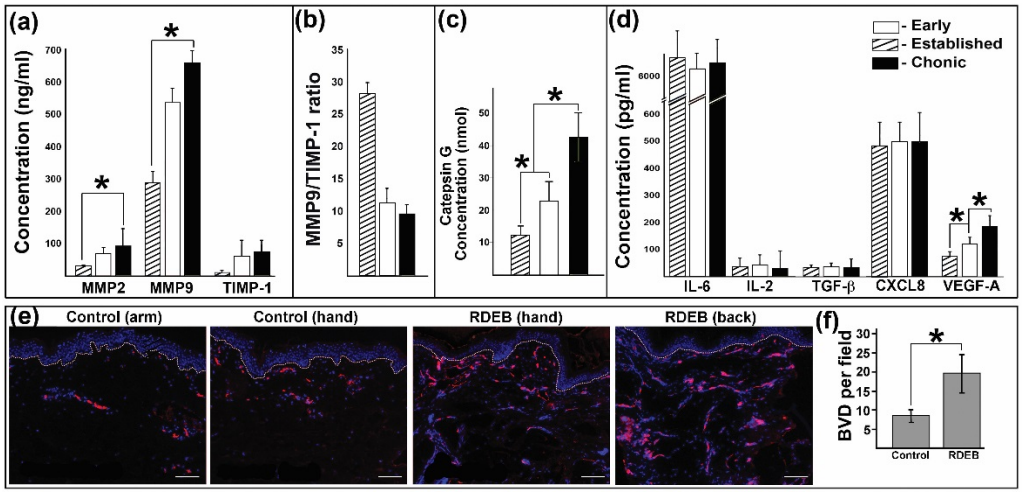

Fig. 4. Evaluation of bandage-recovered soluble factors in early, established and chronic wounds and analysis of angiogenesis in RDEB skin samples. (**a**) ELISA-based quantitation of MMP2, MMP9, and TIMP-1 in a soluble fraction recovered from bandages covering early, established, and chronic wounds. Data are presented as a mean concentration (ng/ml) of triplicate measures ±SD. (**b**) Column chart depicting average MMP9/TIMP-1 ratio in early, established and chronic wounds. Data are presented as fold difference ±SD. (**c**) Column charts showing cathepsin G concentration in early, established and chronic wounds as determined by cathepsin G assay. Data are resented as mean concentration ±SD. (**d**) ELISA-based quantitation of selected cytokines and growth factors (indicated below the columns) in early, established and chronic wounds (as indicated in the key). Data are presented as mean concentration (pg/ml) ±SD. In all column charts, statistical significance ($p<0.05$) is indicated by asterisk. At least, 4 independent samples per wound type per detected protein were used. (**e**) Representative micrographs illustrating elevated number of $CD31^+$ blood vessels in RDEB intact (undamaged) skin. Source of skin samples (genetically normal control and RDEB) are indicated above the micrographs. Red - $CD31^+$ blood vessels; blue - DAPI nuclear staining. The basement membrane zone is outlined by dotted line. Scale bar - 100μm. (**f**) Analysis of blood vessel density (BVD) per section of the skin. Data are presented as an average number of blood vessels per section ±SD. Eight independent control and 23 RDEB samples were used for the assessment. Statistical significance ($p<0.05$) is indicated by asterisk.

Healing of skin wounds depends on different biochemical mediators such as growth factors and cytokines. To evaluate suitability of bandage-derived samples for the analysis of these soluble factors, we also measured interleukin 6 (IL-6) and IL-2, two cytokines known to contribute to wound healing. ELISA-based quantitation showed that both interleukins are present in all examined wounds with IL-6 levels in nanogram range and IL-2 in picogram range (Fig. 4d). No significant difference was detected between the cytokine levels in different wounds. Similarly, there were no significant differences in soluble TGF-β and a pro-inflammatory/pro-angiogenic chemokine CXCL8 (IL-8) in all wound types. Assessment of vascular endothelial growth factor (VEGF)-A), a known angiogenic factor which contributes to normal wound healing, showed significant difference in chronic wounds, as compared to early lesions (Fig. 4d). Because excessive angiogenesis and elevated VEGF levels contribute to hypertrophic scarring, we also examined micro vessel density (MVD) in biopsy samples obtained from 23 RDEB patients and eight controls. Indirect immunofluorescence detection of $CD31^+$ blood vessels showed that RDEB skin has more blood capillaries than normal skin (Fig. 4e, f). Together with high level of pro-angiogenic CXCL8 and elevated VEGF-A in chronic wounds, these findings suggest that increased angiogenesis in RDEB skin may contribute to poor wound healing and hypertrophic scarring of the skin.

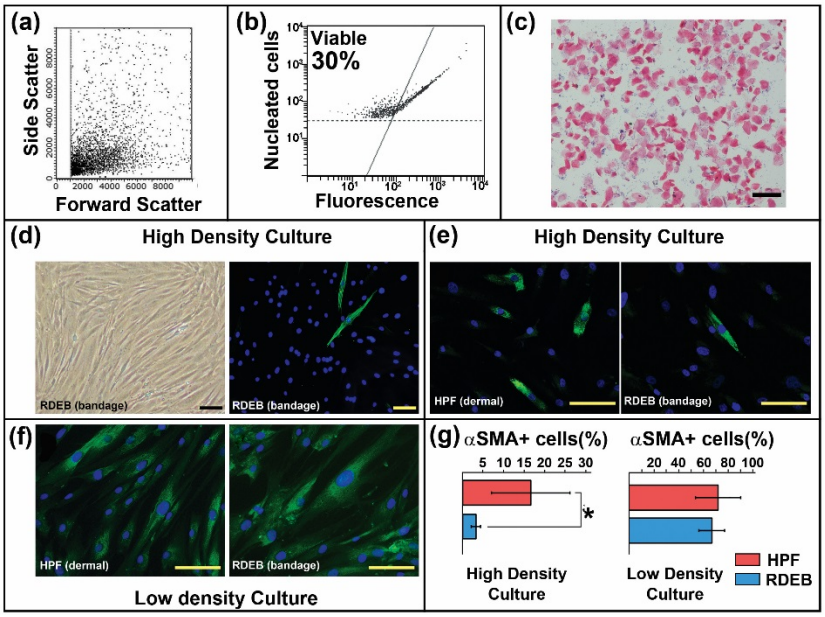

Fig. 5. (**a**) Representative dot-plots illustrating lack of distinct cellular populations recovered from dry or older bandages as defined by FACS-based assessment of side scatter/forward scatter. (**b**) Representative dot-plot illustrating diminished (30% average) viability of cells recovered from dry or older bandages. (**c**) Representative micrograph of the H&E-stained population of cells predominantly containing anucleated keratinocytes (population II in Fig. 1a). These cells lack attachment to plastic substrata. (**d**) Representative micrographs illustrating outgrowth of fibroblastic cells from bandage-recovered cells (population III in Fig.1a) and diminished differentiation into αSMA-producing myofibroblasts when maintained in high-density cultures. (**e**) Representative micrograph illustrating low degree of myofobroblastic (αSMA^+) differentiation of RDEB bandage-derived fibroblasts and significantly higher differentiation of human primary dermal fibroblasts (HPF) maintained in high-density cultures. (**f**) Representative micrograph depicting elevated myofobroblastic (αSMA^+) differentiation of both HPF and bandage-derived fibroblasts maintained in low-density culture. (**g**) Quantitation of αSMA-producing HPF and RDEB myofibroblasts maintained in low and high-density cultures, as indicated in the key. Data are presented as average percentage of αSMA^+ cell per microscopic field ±SD. Data were acquired by quantifying αSMA^+ cells on at least 5 random high-power microscopic fields using low-density and high-density fibroblast cultures from wound-covering bandages (n=5) and HPF (n=2). Statistical significance ($p<0.05$) is indicated by asterisk. On panels: Blue – DAPI nuclear staining; Green – αSMA^+ cells. Scale bar – 100 μm.

<u>*Subtask 2:*</u> Analysis of neutrophils in EB wounds. Timeline - 6 months (18-24).
<u>*Per SOW:*</u> Neutrophil functionality in healing and non-healing EB wounds will include neutrophil morphology, apoptosis, phagocytic capacity, production of proteases and anti-microbial peptides using various assays.
<u>*Progress:*</u> These studies were postponed due to COVID-19, and are currently underway.

<u>*Subtask 3:*</u> Assessment of fibrocytes at wound sites. Timeline - 6 months (18-24).
<u>*Per SOW:*</u> Fibrocyte dynamics in healing and non-heling wounds will be characterized by FACS using sub-type specific markers; fibrocyte-secreted pro-inflammatory mediators will be evaluated by Multiplex-based multi-analyte ELISAs; TLR4 activation by fibrocyte-derived DAMPs will be analyzed by Western blot, RT-PCR and ELISA assays.
<u>*Progress:*</u> Bandage-recovered cells associated with population III (Fig. 1a) were able to produce fibroblastic cell cultures (fibrocytes), which differentiate into alpha smooth muscle actin (αSMA) expressing cells when maintained as a sparse culture (Fig. 5d-g). Wound healing is a complex process involving numerous molecular and physiological pathways. Under normal conditions a normal balance between deposition and degradation of extracellular matrix (ECM) molecules, including collagens and fibronectin, characterizes the synchronized wound healing process. This precisely maintained balance is altered in

chronic wounds. Fibrosis has been implicated in the healing process and an accumulation of profibrotic molecules such as various collagens and a reduction of antifibrotic molecules such as metalloproteinases are part of this process. Therefore, it is essential to study the fibrotic process as a crucial component of normal and pathological wound healing. In this study, we analyzed the amounts of various ECM proteins present in the exudates of skin wounds from EB patients at three wound stages: early, established, and chronic wounds. We performed Western blot analysis of collagens type I and III, fibronectin, and fibronectin EDA for the comparative analysis of early, established, and chronic wound exudates from six EB patients. Owing to its recently recognized role in the establishment of tissue fibrotic reactions, additional Western blot analysis of COMP (cartilage oligomeric matrix protein) was performed. Exudate fractions were obtained and 30 μg of total protein was loaded into 3-8% Tris-Acetate gels, followed by transfer to nitrocellulose membranes using iBlot and then blocked for 1 h at room temperature in blocking buffer. The antibodies against specific ECM proteins were added and incubated with the blots overnight. The detection of the proteins recognized by specific antibodies was performed employing IDRye 800CW anti-goat or anti-rabbit, and IDRye 680RD anti- mouse antibodies. The intensity of the bands was measured employing the Odissey IR reader and the values were represented in a bar graph as relative concentrations to the value obtained from early wounds (arbitrary units). The results showed a marked reduction of bands corresponding to intact collagen type I with the worsening status of the wound (Fig. 6a). In contrast, bands corresponding to collagen type III did not display any common pattern that provided any clear conclusion. Regarding Fibronectin or FN-EDA proteins, these studies demonstrated a tendency to increased levels of FN and, more importantly, of FN-EDA in chronic wounds comparing to early of established wounds, although the values of the differences were not statistically significant (Fig. 6b). Of particular relevance, however, we found a remarkable increase in the degradation of fibronectin in every analyzed exudates; therefore, the data shown were obtained adding the amounts of all degraded fibronectin fragments. In contrast with the inconclusive results obtained with the analysis of collagens and fibronectin, we found remarkable results in the levels of COMP, an ECM molecule recently implicated playing an important role in the fibrotic process. We found that the amount of COMP present in the exudates was markedly decreased, and was even absent in chronic wounds compared with early or established wounds (Fig. 6c). Taken together, these results demonstrate that the fibrotic process that occurs in normal wound healing is altered in skin wounds from EB patients. The finding of decreasing amounts of the most abundant collagen in the dermis (collagen type I) that is also the major collagen involved in wound healing, accompanied by the remarkable degradation of fibronectin and fibronectin EDA indicate that both a higher proteolytic process coupled with a reduction of ECM protein

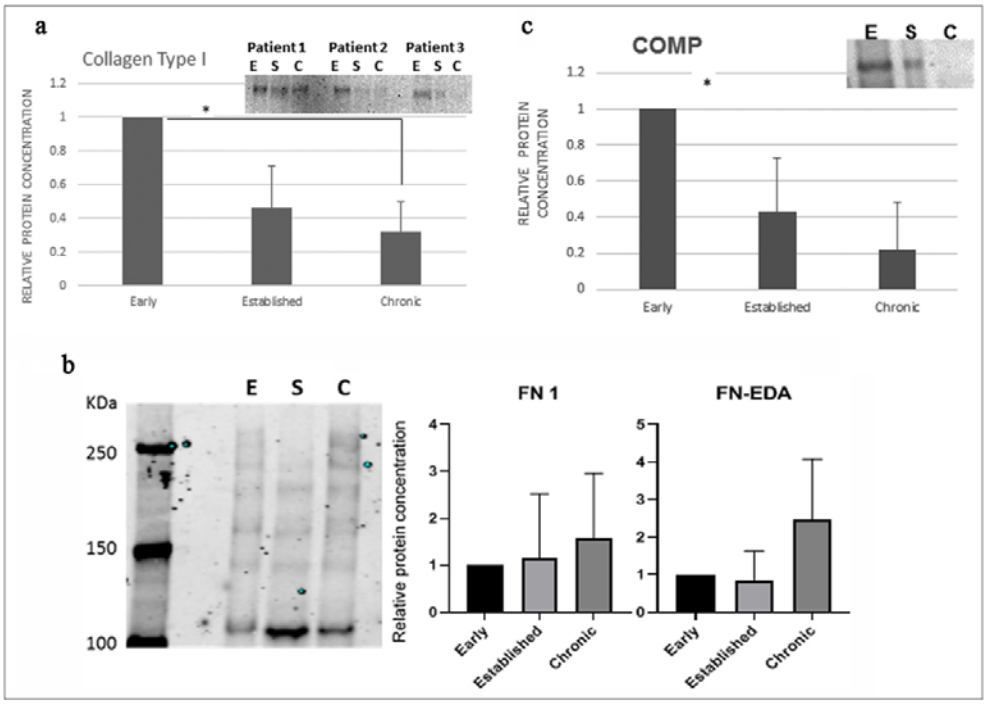

Figure 6. (a) Relative collagen type I protein concentration in the exudates of various wounds from EB patients by Western Blot analysis. E: Early; S: Established; C: Chronic wounds. *p 0.02. (b) Western blot of FN from exudate of one of EB patient. E: Early; S: Established; C: Chronic wounds. B. Relative Fibronectin (FN) and FN-EDA concentration analysis in the exudates of various wounds from EB patients by Western Blot analysis. The observed differences were not statistically significant. (c) Relative COMP protein concentration in the exudates of various wounds from EB patients by Western Blot analysis. E: Early; S: Established; C: Chronic wounds. *p 0.005; **p 0.001. The insert shows a representative Western blot from exudate samples from one EB patient.

production are responsible for this unbalance. Of particular interest is the remarkable reduction of COMP levels in the most severe wounds. These observations open a new field in the research of potential biomarkers for the wound healing process and identify a novel target for therapeutic interventions for severe chronic wounds in EB patients.

Milestone(s) Achieved: Timeline - 24 month. A well characterized analysis of cellular infiltrates of EB-associated wounds. Acquisition of statistically significant data. All tasks except *Subtask 2* are accomplished, manuscript under review.

Specific Aim 2. To characterize microbial dynamics and immunogenicity of the wound colonizing bacteria.

Major Task 3: Analysis of bacterial microbiome in new, established and chronic wounds.

Subtask 1: Sample collection. Timeline - 12 months (1-16).
Per SOW: Wound swabs will be collected concurrently with wound-dressing bandages during routine re-dressing of the wounds at Dr. Salas's clinique using the Levine non-invasive technique. Demographic data, EB type, age of the wound/blisters will be collected by attending physicians at Dr. Salas's clinique. At least 40-50 patients with each type of wound (fresh, established or chronic) will be used for bacterial microbiome studies.
Progress: All samples were collected concurrently with bandages.

Subtask 2: Sample processing and analysis. Timeline - 12 months (13-24).
Per SOW: DNA isolation and sequencing using the Illumina MiSeq platform will be done at the CHOP microbiome Center as a service. Data analysis will be done using R Statistical Package as well as non-parametric Wilcoxon rank-sum tests, Spearman correlations and Kruskal-Wallis tests for all computations.
Progress: Due to COVID-19, these studies were postponed. During COVID-19 pandemic, the CHOP Microbiome Center was only accepting samples for COVID-19-related projects. Currently, we are waiting for the CHOP Microbiome Center to accept our samples for analysis. It is expected that miSeq and related bioinformatics analyses will be completed by December 2020.

Milestone(s) Achieved: Timeline - 24 month. A well characterized analysis of bacterial communities of EB-associated wounds. Acquisition of statistically significant data. It is expected that miSeq and related analyses will be completed in September-November, 2020.

Major Task 4: Analysis of fungal mycobiome in new, established and chronic wounds.

Subtask 1: Sample collection. Timeline - 12 months (1-12).
Per SOW: Samples collected for microbiome studies will also be used for fugal assessment. At least 40-50 patients with each type of wound (fresh, established or chronic) will be used for fungal studies.
Progress: All samples were collected concurrently with bandages.

Subtask 2: Sample processing and analysis. Timeline - 12 months (13-24).
Per SOW: Partly, DNA extracted for microbiome assessment will be used for fungal mycobiome analysis. The fungal component will be sequenced using the Illumina MiSeq platform at CHOP microbiome Center as a service. The Shannon diversity index, Simpson diversity index (1-Dominance), Faith's phylogenetic distance (PD), and number of observed species (richness) will be calculated using the QIIME 1.8.0 alpha_diversity.py script.
Progress: Due to COVID-19, these studies were postponed. During COVID-19 pandemic, the CHOP Microbiome Center was only accepting samples for COVID-19-related projects. Currently, we are waiting for the CHOP Microbiome Center to accept our samples for analysis. It is expected that miSeq and related bioinformatics analyses will be completed by December 2020.
Milestone(s) Achieved: Timeline - 24 month. A well characterized analysis of fungi communities of EB-associated wounds. Acquisition of statistically significant data. It is expected that miSeq and related analyses will be completed in September-November, 2020.

Major Task 5: Analysis of microbiota immunogenicity and adaptive T cell immunity at wound site.

Subtask 1: Assessment of microbiota-specific T cells in early, established and chronic wounds. Timeline – 12 month (13-18).
Per SOW: Functional profile of bacteria-specific T cells will be evaluated by Multiplex ELISA assays.
Subtask 2: Analysis of the microbiota-induced immunosuppression. Timeline -12 (18-24).
Per SOW: Differentiation and activation of the bandage-derived T cells at different stages of wound progression will be assessed by FACS. Cytokine production and secretion by activated T cells will be analyzed by ELISA and ELISpot assays.

Progress for Subtasks 1 and 2: Staphylococcus aureus is the most common bacteria in RDEB wounds with no active bacterial infection and is a likely target for CTL activity in RDEB skin. To define microbial species whose antigens could be recognized by the adaptive T cell-mediated immunity in RDED wounds with no documented active bacterial infections, we evaluated microbial contaminants in liquid samples, wound-associated epithelial cells, and culture media from wound-derived cultured keratinocytes (KC). This evaluation showed that *Staphylococcus aureus* is detected in 50% of the liquid samples with high, medium, and low levels of contamination as defined by semi-quantitation of the PCR. Fewer samples contained *Staphylococcus epidermidis* and *Pseudomonas aeruginosa* with mostly high and medium levels of contamination. Other most common bacterial and fungal wound contaminants were not detected in all analyzed samples. While evaluating both bandage-derived liquid and cellular fractions, we found that about 60% of samples contained cell-associated *S.aureus*, *S.epidermidis, and P.aeruginosa* with *S.aureus* being a predominant intracellular contaminant. In few cases, *S.aureus* was detected only in cells but not in a corresponding liquid fraction. Furthermore, *S. aureus* was found in conditioned media collected from several samples of cultured cells. These finding demonstrated that this bacteria can infect and survive in KC. Considering this data and prior studies showing the presence of *S. aureus*-derived antigens and super-antigens recognizable by adaptive immunity, it is likely that *S. aureus* could be the primary target for the adaptive immunity, particularly, cytotoxic T lymphocytes (CTL) in RDEB wounds. Unlike viruses, which most often utilize cell surface receptors to infect host cells, bacterial cells are engulfed by the host cells and, using different mechanisms, can survive inside the host. Macrophages and neutrophils are well-equipped for bacterial phagocytosis. However, there are data showing that other cell types, particularly, KC, could be infected by bacteria. Using AlexaFluor^{594}-labeled *S.aureus* we evaluated its ability to infect control and RDEB-derived KC. Initial assessment showed that overnight exposure of the cells to the bacteria leads to a robust infection. Scanning of infected cells at 5μm Z-position using confocal microscopy clearly showed an overwhelming presence of bacterial particles in RDEB RDEB KC as compared to control cells. Quantitation of fluorescence showed that 4h exposure is sufficient for infection, yet, statistically significant difference between control and RDEB cells were seen only after overnight infection. Further analysis showed that *S. aureus* particles are routed inside RDEB KC via Rab7A$^+$ early phagoendosomes and occasionally via LC3$^+$ autophagosomal compartments. Evaluation of the *S. aureus* in control and RDEB intact skin by indirect immunofluorescence showed no significant difference. In control and RDEB skin most of *S. aureus* co-localized with CD11b$^+$ cells in the dermis and was also detected on skin surface. Collectively, based on the current knowledge of the intracellular bacterial trafficking, antigen presentation and our current data, it is plausible that *S. aureus* is a likely candidate for CTL-mediated recognition and killing of infected RDEB KC as well as macrophages and neutrophils, which are well-equipped to engulf bacteria.

Microbial antigen-specific CD4$^+$ and CD8$^+$ T cells are present in RDEB skin wounds. To evaluate whether microbial antigen-specific CD4$^+$ and CD8$^+$ T cells are present in skin wounds of RDEB patients, a pool of CD3$^+$ T cells was isolated from wound-covering bandage-derived leukocytes by positive selection and propagated *in vitro*. FACS-based immuno-phenotyping showed that CD4$^+$ and CD8$^+$ T cells at ratio of 9 to 1, respectively, were present in a total T cell population. After re-stimulation with anti-CD3/CD28 and 2-day period of rest, T cells were exposed to wound-associated pooled microbial antigens. Bandage-derived T cells specifically responded to the antigens by clonal expansion. It was detected by light microscopy after 1 day of exposure and was most profound after 2 days. CFSE dilution assay showed that 2-day exposure to microbial antigens induced robust proliferation in about 30% of patient-derived T cells, and did not appreciably affected proliferation of control cells isolated from PBMC of healthy donors, in which anti-CD3/CD28 stimulation triggered robust

proliferation. Intracellular staining for IFNγ and IL-2 combined with detection of CD107 (degranulation marker) confirmed microbial antigen-specific activation of patient-derived T cells. A significant increase in INFγ-expressing cells was detected in all bandage-derived samples exposed to microbial antigens. Also, there was a specific population of patient-derived T cells strongly responding to the antigens by IFNγ production and degranulation among $CD8^+$ T cells. Some increase in the intracellular IL-2 was detected in $CD4^+$ T cell, but it was marginally elevated as compared to controls. Furthermore, quantitative ELISA showed that INFγ secretion by T cells was induced. Even 1 day of exposure to microbial antigens led to a secretion of about 100 pg/ml of INFγ into culture media, which reached about 275 pg/ml by day 5 of exposure. At the same time, no appreciable changes in IL-2 and IL-17 secretion were detected in media samples. Collectively, these data demonstrated that RDEB wounds contain a pool of primed T cells, which react to microbial antigens by proliferation, degranulation, and secretion of IFNγ.

Wound-derived T cells can recognize S. aureus antigens and target infected keratinocytes in HLA-dependent manner. Considering our findings regarding *S. aureus* in RDEB wounds, and presence of *S. aureus*-specific super antigens recognized by the immune system, we tested the capacity of wound-derived T cells to recognize and target *S. aureus*-infected KC. To set-up IFNγ ELISpot assay, available RDEB KC and RDEB patient-derived T cells were screened by FACS for the HLA-A2.1 expression and $HLA\text{-}A2.1^+$ allogeneic cells were used for experiments. Incubation of either control healthy donor-derived or patient-derived T cells with heat-inactivated *S. aureus* did not lead to T cell activation and IFNγ secretion. Small number of spot-forming cells (SFC) was detected when T cells were exposed to uninfected KC. Exposure of T cells to pooled RDEB bandaged-derived microbial antigens showed an elevated T cells response, yet, the difference was not significant. Much higher number of SFC was detected when RDEB-derived T cells were incubated with *S. aureus*-infected RDEB KC. Although some control T cells were activated by exposure to infected KC, the difference between control and RDEB T cell responses was significant. Because $CD8^+$ T cells were identified among microbial antigen responders, the presence of CTL capable of targeting and killing infected KC among RDEB-derived T cells was evaluated by standard FACS-based CTL assay. Assessment showed a significantly higher CTL activity in all examined RDEB T cell pools exposed to infected KC as compared to uninfected cells. Moreover, it appears that CTL response against infected KC is HLA-restricted. Cytotoxicity against *S. aureus*-infected KC was further validated by granzyme B activity assay, which showed a significantly higher granzym B activity release by RDEB-derived T cells following exposure to infected KC. Collectively these data demonstrated that *S. aureus*-specific memory/effector T cells capable of targeting and killing infected cells are present in RDEB wounds.

PD-1 and Treg-dependent mechanisms may contribute to bacteria-specific T cells exhaustion in chronic wounds. In chronic infections, which are commonly observed in RDEB patients, T cell exposure to a persistent antigenic load could be associated with down-modulation of robust effector functions, expression of different inhibitory receptors, and T cell exhaustion. Short-term (4 h) exposure of RDEB T cells to the pooled RDEB wound-derived microbial antigens led to a transient induction of CD69 in about 50% of $CD4^+$ and 15% of $CD8^+$ RDEB-derived T cells. It was accompanied by induction of PD-1 on 15% of $CD4^+$. As expected, longer incubation diminished CD69 expression but led to an induction of PD-1 expression in up to 38% of $CD4^+$ T cells. PD1 expression was not appreciably changed on $CD8^+$ T cells. Expression of CD57, a markers of T cell exhaust, was not induced by prolong up to 1 week exposure. Considering these data, it likely that 1 week exposure of RDEB T cells to RDEB-derived pooled microbial antigens does not trigger T cell exhaust *in vitro*, yet, higher percentage of antigen-exposed $PD\text{-}1^+CD4^+$ T cells suggests that down-modulation of effector T cell function could be triggered in PD-1-dependent manner. Since immune-inhibitory activity of regulatory T cells (Treg) may also play a role in diminishing T cell-mediated response to bacterial antigens, we also evaluated $CD25^+FOXP3^+$ cells in a population of bandage-derive lymphocytes. All examined samples demonstrated the presence a distinct population of Treg cells, which corresponded to about 10% of total T cells, regardless of wound type. These data suggested that Treg cells may also play a role in down-modulating T cell effector function in RDEB wounds.

Milestone(s) Achieved: Timeline - 24 month. A well characterized role of T cell immunity in controlling microbiota in EB-associated wounds. All tasks are accomplished, manuscript in preparation.

5. OPPORTUNITIES FOR TRAINING AND PROFESSIONAL DEVELOPMENT
Nothing to report

6. IMPACT
It is anticipated that the proposed analyses will allow us to define precipitating factors, which predefine abnormal wound healing in EB skin lesions. In the short term, these investigations will allow us to develop clinically relevant tests and algorithms to assess wound healing capacities of the EB-associated wounds. Analysis of the microbiome and concurrent cellular infiltrates will also permit better selection of antibiotic and antiseptic creams/ointments to restore microbiota balance and decrease inflammatory response. In the long term, the obtained data will pave the path to the development of novel therapeutic approaches aimed at prevention and management of chronic wounds focused on reduction of inflammation and fibrosis.

7. CHANGES/PROBLEMS
Due to COVID-19 situation, we encountered several delays in accomplishing following tasks:

Major Task 2: Cross-sectional and longitudinal analyses of cellular infiltrates in EB healing and non-healing wounds.
Subtask 2: Analysis of neutrophils in EB wounds. Timeline - 6 months (18-24).

Major Task 3: Analysis of bacterial microbiome in new, established and chronic wounds.
Subtask 2: Sample processing and analysis. Timeline - 12 months (13-24).

Major Task 4: Analysis of fungal mycobiome in new, established and chronic wounds.
Subtask 2: Sample processing and analysis. Timeline - 12 months (13-24).

Action Plan:

- Studies of EB-associated neutrophils are underway. It is expected to complete these studies by December 2020.
- During COVID-19 pandemic, the CHOP Microbiome Center was only accepting samples for COVID-19-related projects. Currently, we are waiting for the CHOP Microbiome Center to accept our samples for analysis. It is expected that miSeq and related bioinformatics analyses will be completed by December 2020.

8. PRODUCTS
"Aberrant recruitment of leukocytes defines poor wound healing in patients with recessive dystrophic epidermolysis bullosa". Taylor Phillips, Leonie Huitema, PhD[1#], Rodrigo Cepeda, Diego de los Cobos, Regina Isabella Matus Perez, Mauricio Salas Garza, Franziska Ringpfeil, Bahar Dasgeb, Jouni Uitto, Julio Cesar Salas-Alanis, Vitali Alexeev, Olga Igoucheva, Under 1st revision, *Journal of Dermatological Science*, 2020

"Intracellular escape strategies of *Staphylococcus aureus* in persistent cutaneous infections". Leonie Huitema, Taylor Phillips, Vitali Alexeev, Marjana Tomic-Canic, Irena Pastar, Olga Igoucheva, Under review, *Experimental Dermatology*, 2020

"T cell activation and bacterial infection in skin wounds of patients affected by recessive dystrophic epidermolysis bullosa". Leonie Huitema, Eric Saukaitis, Taylor Phillips, Diego de los Cobos, Regina Isabella Matus Perez, Franziska Ringpfeil, Bahar Dasgeb, Gudrun Debes, Jouni Uitto, Julio Cesar Salas-Alanis, Vitali Alexeev, Olga Igoucheva. Manuscript *in preparation*.

9. PARTICIPANTS AND OTHER COLLABORATIG ORGANIZATIONS

What individuals have worked on the project?

Name:	Olga Igoucheva	Vitali Alexeev	Leonie Huitema	Taylor Phillips
Project Role:	Principal Investigator	Co-Investigator	Research Associate	Research Technician
Researcher Identifier (ORCID ID):	https://orcid.org/0000-0001-9813-7184	https://orcid.org/0000-0002-0762-1833	https://orcid.org/0000-0003-2947-021X	https://orcid.org/0000-0001-9843-4736
Nearest person month worked:	11	6	12	12
Contribution to Project:	Dr. Igoucheva supervised all aspects of the study and performed FACS and Legend Plex analyses of patient-derived samples	Dr. Alexeev was involved in all aspects of the Aims 1 and 2, including analysis of bandage-derived cells and T cell-mediated immunity	Dr. Huitema was involved in all aspects of the Aims 1 and 2, including analysis of bandage-derived cells and T cell-mediated immunity	Ms. Phillips was involved in studies related to leukocytic infiltrates, T cell- mediated immunity and maintenance of mouse colony for studies outlined in Aim 3as well as maintenance of the laboratory
Funding Support:	None	Hasumi Research Fund	No change	No change

Has there been a change in the active other support of the PD/PI(s) or senior/key personnel since the last reporting period?

Dr. Chervoneva's previously active R01-CA196278, Dr. Ralph and Marian Falk Medical Research Trust grant and two NIH subawards have ended, and her previously pending R01CA18263 and one NIH subaward have become active.

Dr. Uitto's previously pending NIH subaward has become active.

What other organizations were involved as partners?

No other organizations were involved as partners.

10. SPECIAL REPORTING REQUIREMENTS

Nothing to report

11. APPENDIECIES

Nothing to report